Bioconjugate Chemistry

pubs.acs.org/bc Article

Covalently Immobilizing Interferon-γ Drives Filopodia Production through Specific Receptor−Ligand Interactions Independently of Canonical Downstream Signaling

Shaun M. Christie,[‖] Trevor R. Ham,[‖] Grant T. Gilmore, Paul D. Toth, Nic D. Leipzig,* and Adam W. Smith*

Cite This: *Bioconjugate Chem.* 2020, 31, 1362−1369 Read Online

ACCESS | Metrics & More | Article Recommendations | Supporting Information

ABSTRACT: Immobilizing a signaling protein to guide cell behavior has been employed in a wide variety of studies. This approach draws inspiration from biology, where specific, affinity-based interactions between membrane receptors and immobilized proteins in the extracellular matrix guide many developmental and homeostatic processes. Synthetic immobilization approaches, however, do not necessarily recapitulate the *in vivo* signaling system and potentially lead to artificial receptor−ligand interactions. To investigate the effects of one example of engineered receptor−ligand interactions, we focus on the immobilization of interferon-γ (IFN-γ), which has been used to drive differentiation of neural stem cells (NSCs). To isolate the effect of ligand immobilization, we transfected Cos-7 cells with only interferon-γ receptor 1 (IFNγR1), not IFNγR2, so that the cells could bind IFN-γ but were incapable of canonical signal transduction. We then exposed the cells to surfaces containing covalently immobilized IFN-γ and studied membrane morphology, receptor−ligand dynamics, and receptor activation. We found that exposing cells to immobilized but not soluble IFN-γ drove the formation of filopodia in both NSCs and Cos-7, showing that covalently immobilizing IFN-γ is enough to affect cell behavior, independently of canonical downstream signaling. Overall, this work suggests that synthetic growth factor immobilization can influence cell morphology beyond enhancing canonical cell responses through the prolonged signaling duration or spatial patterning enabled by protein immobilization. This suggests that differentiation of NSCs could be driven by canonical and non-canonical pathways when IFN-γ is covalently immobilized. This finding has broad implications for bioengineering approaches to guide cell behavior, as one ligand has the potential to impact multiple pathways even when cells lack the canonical signal transduction machinery.

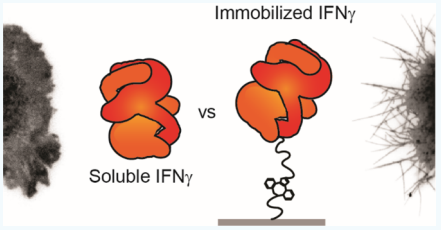

INTRODUCTION

The interaction of signaling proteins and cell surface receptors guides a variety of different cell processes and behaviors. Downstream activation cascades are driven by receptor oligomerization or post-translational modifications following these binding events.[1] The strategy of immobilizing signaling proteins to control this activation has been employed in a wide variety of applications, including but not limited to lineage specification,[2−5] guidance cues,[6−8] or adhesion.[9,10] Protein immobilization draws inspiration from biology, as the body often sequesters growth factors or guidance cues to the extracellular matrix (ECM, e.g., using heparin-binding domains),[11] providing latent instructions to cells with precise control over their presentation. However, many techniques for synthetic protein immobilization do not entirely recapitulate this process. Proteins which would naturally only be available in soluble form (e.g., chemokines) can be immobilized and may show greatly enhanced potency and signaling duration. Importantly, proteins which are immobilized using a covalent bond (e.g., strain-promoted azide−alkyne cycloaddition, SPAAC)[2] presumably remain in place after receptor binding and the receptor−ligand complex cannot be internalized in a natural manner. Likewise, the diffusion of membrane-bound receptors is certainly altered after binding an immobilized ligand. Ultimately, both receptor−ligand interactions and signal transduction/regulation are perturbed by immobilizing a protein ligand, but little is known regarding how this affects direct downstream signaling and cellular responses.

Interferon-γ (IFN-γ) has been shown to play a role in neural differentiation and survival,[12] among other areas.[13] Its receptor complex consists of two ligand binding chains (interferon-γ-receptor 1, IFNγR1) and two signal transduction chains (interferon-γ-receptor 2, IFNγR2).[13] IFN-γ is a constitutive homodimer and binds IFNγR1 in a 2:2 binding stoichiometry. Upon ligand binding, a conformational change in the receptor complex causes a signaling cascade which results in the

Received: February 24, 2020
Revised: April 22, 2020
Published: April 24, 2020

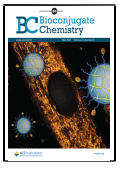

https://dx.doi.org/10.1021/acs.bioconjchem.0c00105
Bioconjugate Chem. 2020, 31, 1362−1369

phosphorylation of signal transducer and activator of transcription 1 (STAT1).[13−16] We have previously immobilized recombinant, N-terminally azide-tagged IFN-γ and observed key differences in neural stem cell (NSC) behavior when exposed to immobilized or soluble forms.[2,4,17] Here, we sought to characterize immobilized IFN-γ signaling in more detail and understand how it likely differs from soluble signaling regarding the pathways involved and the morphological response of the cell.

We first isolated NSCs from 6−8-week-old female Fisher 344 rats and observed robust filopodia production when exposed to immobilized IFN-γ. We then transiently transfected Cos-7 cells to express IFNγR1-GFPSpark but not IFNγR2, meaning that they could bind the ligand but not undergo canonical signal transduction, and found the same increase in filopodia. We investigated the effect of immobilizing IFN-γ on receptor−ligand specificity and downstream signaling using a combination of fluorescent fluctuation spectroscopy and immunofluorescent (IF) imaging. Overall, we have determined that the morphological response results from the immobilization itself and does not require the presence of the full signaling complex used in canonical IFN-γ signaling pathways.

RESULTS AND DISCUSSION

Immobilizing IFN-γ Drives Filopodia Formation in NSCs. To visualize the cellular response when signaling proteins are covalently immobilized to a surface, we began by looking at NSC morphology after a 4 h exposure period to immobilized IFN-γ (Figure 1 and Figure S1). Total internal reflection fluorescence (TIRF) imaging showed the number of NSCs that produced a large amount of filopodia when exposed to immobilized IFN-γ was increased by 2-fold compared to the control surface (no IFN-γ, Figure 1). NSCs possess the full signal transduction machinery for IFN-γ and are known to undergo neuronal differentiation following exposure to both soluble and immobilized IFN-γ.[2−4,12,18−22] Generation of filopodia is involved in sensing matrix-bound cues during neural patterning and guidance,[23] but the connection between the immobilized ligand−receptor interaction and this morphological response is unclear.

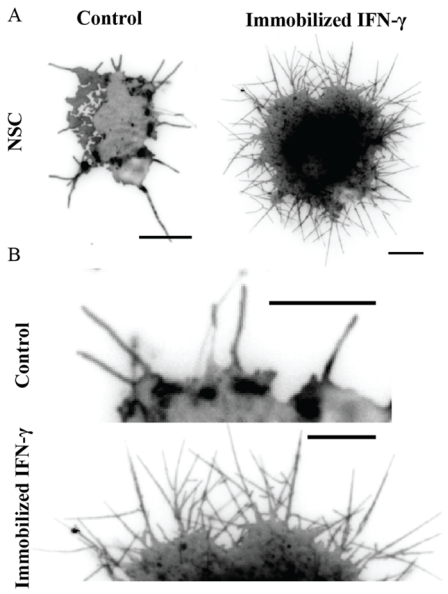

Figure 1. NSCs produce filopodia in response to immobilized IFN-γ. (A) Representative TIRF images of live primary rat NSCs stained with DiO-C18 (a membrane incorporating dye) following incubation on control (no IFN-γ) surfaces (n = 100) or immobilized IFN-γ surfaces (n = 160). NSCs on immobilized IFN-γ produce a large amount of filopodia compared to the control surface. See Figure S1 for additional images. Scale bars represent 10 μm. (B) Close-up of the cell edge showing filopodia in detail. Filopodia on control surfaces are sparse, and incubation on immobilized IFN-γ surfaces produces overlapping structures.

Immobilizing IFN-γ Drives Filopodia Formation in IFNγR1-Expressing Cos-7. We next investigated whether immobilized IFN-γ could induce a similar morphological change in cells without the canonical signal transduction machinery. A model Cos-7 cell line was used for efficient transient transfection of IFNγR1, without IFNγR2, so they could bind the ligand but not transduce the signal.[13] Cos-7 cells are an easily cultured fibroblast-like kidney cell line from the African green monkey that normally adopt a round, symmetric morphology without filopodia (Figure 2A, left column).[24] When exposed to immobilized but not soluble IFN-γ over 4 h (Figure 2), filopodia appear at the cell edges. Without overlapping filopodia, we were able to quantify filopodia production using the recently developed ImageJ plugin, Filoquant, allowing semi-automated detection using TIRF images (changes to default parameters are described in the Experimental Procedures).[25,26] Exposure to soluble IFN-γ did not result in a change in average filopodia number or qualitative cell morphology when compared to the control cells (Figure 2A,C), although it did result in a slightly longer cell edge compared to control cells (Figure 2D, $p < 0.01$). Exposure to immobilized IFN-γ resulted in robust filopodia formation (Figure 2B), both in terms of total filopodia per cell (Figure 2C, $p < 0.0001$) and the total cell edge length (Figure 2D, $p < 0.0001$), which indicates greater adherence.[27] Additionally, we observed an increase in the average length of filopodia after stimulation with immobilized IFN-γ (Figure S2A, left, $p < 0.0001$). Figure S2B shows that control cells tend to have more filopodia only as their cell edge length increases; this trend is not seen during exposure to immobilized IFN-γ, where cells of any size have robust filopodia production.

We next sought to characterize these filopodia over time and observe the differences in filopodia retention between immobilized IFN-γ, adsorbed IFN-γ, or a control surface (no IFN-γ). Representative time-lapse images for each group are shown in Figure 3. For the adsorbed IFN-γ, the cyclooctyne moiety is not present, meaning that any IFN-γ will not be covalently bound. Modest filopodia formation occurs following exposure to adsorbed IFN-γ, but the filopodia quickly retracted over short intervals (Figure 3, middle) in a pulsatile manner. The cells exposed to immobilized IFN-γ retained individual filopodia for the majority of the collection window (Figure 3, bottom), with typical filopodium lifespans of 30+ min. The control cells did not send out significant filopodia over any time scale, and filopodia formation was not dependent on cell density (Figure 3, top). Again, without the full signaling complex present, these IFNγR1-expressing cells display a distinct difference in filopodia response based on the surface properties. The differences in filopodia retention between adsorbed and immobilized IFN-γ indicate that the mechanism of attachment plays a substantial role, as covalently attaching IFN-γ affected filopodia retention more than simple adsorption. The adsorbed ligand is not covalently bound; therefore, it can be internalized or moved by the receptor

https://dx.doi.org/10.1021/acs.bioconjchem.0c00105
Bioconjugate Chem. 2020, 31, 1362−1369

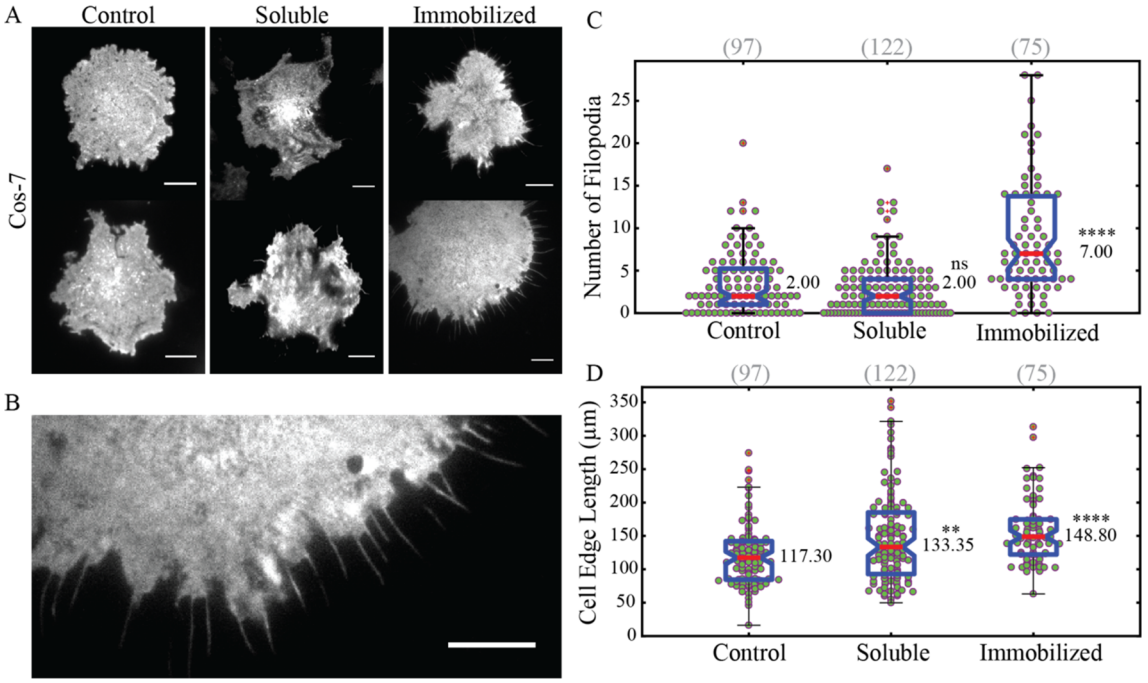

Figure 2. IFNγR1-expressing Cos-7 cells generate filopodia in response to IFN-γ immobilization. (A) TIRF imaging of live Cos-7 transiently transfected with IFNγR1-GFPSpark following incubation on control (no IFN-γ) surfaces, with soluble ligand, or on immobilized IFN-γ surfaces. Exposure to immobilized IFN-γ induces a pronounced increase in filopodia production. Scale bars represent 10 μm. (B) Close-up of the cell edge on a surface containing immobilized IFN-γ, showing filopodia in detail. The scale bar represents 10 μm. (C) Number of filopodia on individual cells quantified using Filoquant[25,26] and represented by a bee swarm plot and box and whisker plot overlay; the red line indicates the median of the data. Exposure to immobilized IFN-γ yields a significantly larger number of filopodia per cell. **** represents $p < 0.0001$, as determined by Student's t test in pairwise comparisons with the control group. (D) Cell edge length (in μm) of individual cells quantified and represented in the same manner as part C. Both soluble and immobilized IFN-γ produce a longer cell edge than cells on control surfaces, with immobilized IFNγ being the highest. ** represents $p < 0.01$ and **** represents $p < 0.0001$, as determined by Student's t test in pairwise comparisons with the control group. The gray numbers above each plot indicate the number of individual cells analyzed. Additional data can be found in Figure S2.

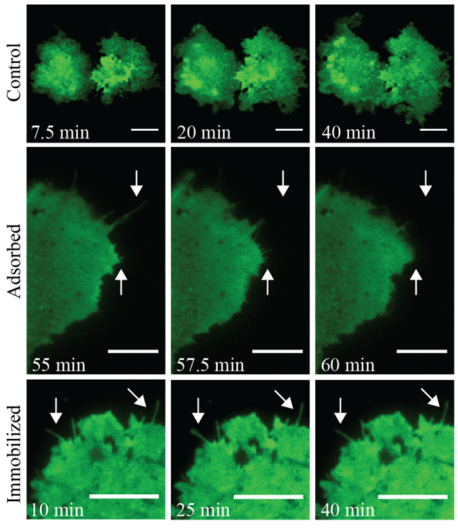

Figure 3. Immobilizing IFN-γ causes IFNγR1-expressing Cos-7 to retain their individual filopodia for longer time scales. TIRF time-lapse imaging of Cos-7-expressing IFNγR1-GFPSpark grown on control (no IFN-γ), adsorbed IFN-γ, or immobilized IFN-γ surfaces. White arrows show filopodia of interest that form and retract in the adsorbed control but are retained with immobilization of IFN-γ. Each time-lapse is obtained at the same magnification and cropped to the region of interest, with scale bars in each panel representing 10 μm.

binding. However, when IFN-γ is covalently bound to the cyclooctyne moiety, the filopodia are retained possibly as an adhesive point due to the immobilized ligand binding, which is discussed below.

Due to their transfection with only part of the canonical signal transduction machinery for IFN-γ, we expected these Cos-7 cells to exhibit no morphological response to IFN-γ. This was the case with soluble IFN-γ, where IFNγR1-expressing Cos-7 cells did not demonstrate any morphological changes. However, exposure to immobilized IFN-γ resulted in robust, persistent filopodia production. The observation of morphological changes in IFNγR1-expressing Cos-7 cells following exposure to immobilized IFN-γ was unexpected and shows that immobilizing a signaling protein can drive cell morphology changes, in addition to the increased persistence and potency of signal for the specific ligand. To investigate this further, we next evaluated the interaction of azide-tagged IFN-γ with IFNγR1.

Fluorescence Fluctuation Spectroscopy Confirms Specific Ligand−Receptor Interaction. To determine if IFN-γ was interacting specifically with IFNγR1 or whether there was a nonspecific response, we used fluorescence fluctuation spectroscopy. We stimulated IFNγR1-GFPSpark-expressing Cos-7 with soluble IFN-γ labeled with 5(6)-carboxy-X-rhodamine. Fluorescence images show that both the receptor and ligand are located at the plasma membrane (Figure 4A). Single-color fluorescence correlation spectroscopy (FCS) was performed on individual cells expressing IFNγR1-GFPSpark, at a surface density between 100 and 1500 molecules/μm^2, before and after ligand binding. From the GFPSpark auto-correlation data, we calculated the

https://dx.doi.org/10.1021/acs.bioconjchem.0c00105
Bioconjugate Chem. 2020, 31, 1362−1369

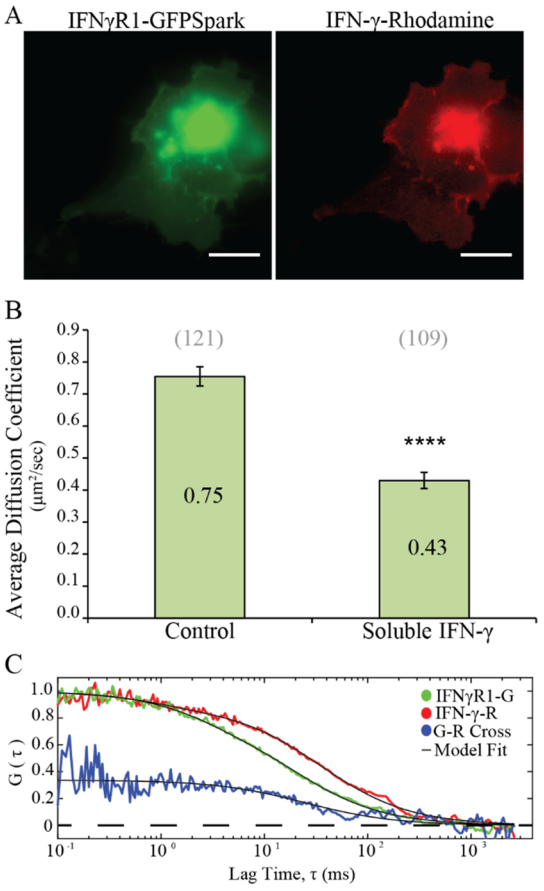

Figure 4. IFNγR1 and azide-tagged IFN-γ interact specifically. (A) Representative Cos-7 cell epifluorescence when transiently transfected with IFNγR1-GFPSpark and stimulated with soluble IFN-γ-rhodamine. Scale bars represent 10 μm. (B) Average diffusion coefficient of IFNγR1 for control and soluble IFN-γ-stimulated Cos-7 cells. During stimulation, diffusion decreases, indicating larger molecular size and complex formation. The gray numbers above each plot represent the number of individual cells analyzed. **** represents $p < 0.0001$, as determined by Student's t test. (C) Typical auto- and cross-correlation curves for azide-tagged IFN-γ-stimulated cells. Average f_c value for IFNγR1-soluble IFN-γ cross-correlation is 0.34 (n = 31), indicating formation of a receptor−ligand complex. See Figure S3 for additional correlation curves.

diffusion coefficient to assess the mobility of IFNγR1 before and after stimulation with soluble IFN-γ. Prior to stimulation, the average diffusion coefficient was 0.755 $\mu m^2/s$, which is consistent with transmembrane proteins measured in these cells in previous studies.[28,29] After exposure to soluble IFN-γ (Figure 4B), the average diffusion coefficient was 0.430 $\mu m^2/s$, indicating reduced mobility due to ligand binding and complex formation beyond a simple dimer.[30] The IFNγR1-GFPSpark diffusion coefficient 4 h after treatment was 0.747 $\mu m^2/s$, which is similar to the diffusion coefficient prior to stimulation, suggesting internalization of the receptor−ligand complexes or dissociation of the ligand (K_D = 0.1 nM, data not shown).[13,16] We used dual color fluorescence cross-correlation spectroscopy (FCCS) of IFNγR1-GFPSpark and IFN-γ-rhodamine for the measurement of receptor−ligand codiffusion. The amplitude of the cross-correlation function is proportional to the degree of binding between the ligand and receptor and is reported as the parameter f_c, which is the ratio of the amplitudes of the cross-correlation function (CCF) and auto-correlation function (ACF).[31] The average fraction correlated for IFNγR1 and soluble IFN-γ was 0.34, signifying the presence of receptor−ligand binding. While there have been reports regarding nonspecific interactions of IFN-γ with lipid membranes,[32] they may be minor, as the FCS and FCCS data here show that cells transfected with IFNγR1 (but not IFNγR2) can still interact specifically with soluble IFN-γ. When the FCS experiments were attempted with immobilized IFN-γ, we observed a sharp decrease in the fluorescence intensity consistent with photobleaching. Photobleaching occurred for both the ligand and receptor, consistent with specific receptor−ligand binding (data not shown).

IFN-γ Immobilization Does Not Activate Canonical Signaling Pathways or Generate Focal Adhesions. Having established that IFN-γ/IFNγR1 interactions were specific under both soluble and immobilized stimulation conditions, we next investigated two explanations for filopodia generation: canonical signaling (i.e., phosphorylation of STAT1) and the generation of focal adhesions. First, since these Cos-7 cells were only transfected to express IFNγR1 and not IFNγR2, we did not expect STAT1 phosphorylation to occur following ligand binding. We note here that during the fixation and staining protocol the filopodia detached from the glass and may have been damaged, so they cannot be quantified in this set of experiments.[33] We verified with IF that no significant STAT1p was observed under any conditions (no IFN-γ, soluble IFN-γ, or immobilized IFN-γ) after 4 h (Figure 5, left). As expected, stimulation of NSCs with IFN-γ resulted in changes to STAT1p localization under both conditions (Figure 5, right). Therefore, in Cos-7 cells, STAT1 does not act as the transcription factor for filopodia production in this immobilized IFNγ-IFNγR1 induced pathway.

As cells protrude and/or migrate (e.g., neuronal pathfinding or angiogenesis),[23,34] they use filopodia to sense their environment and guide this process. While the full mechanisms and purpose are not known,[35] there is evidence that adherent focal complexes within filopodia guide the generation of focal adhesions (FAs) and, in turn, the manner in which cells adhere and direct their protrusions.[36] One plausible mechanism for filopodia generation in IFNγR1-expressing Cos-7 cells was that sustained receptor−ligand binding and immobilization stimulated an alternate signaling pathway (i.e., integrin mediated adhesion) and replicated this process.[37] To determine whether immobilized IFN-γ was encouraging filopodia formation in such a manner, we stained for actin (using fluorescently labeled phalloidin) and vinculin (using IF) to assess FA production (Figure 6). We found that IFNγR1-expressing Cos-7 cells formed FAs on collagen-coated surfaces as expected (Figure 6, bottom, arrows indicate vinculin localization at the ends of actin stress fibers). However, stimulation with soluble or immobilized IFN-γ showed no increase in FA generation relative to control cells, indicating that altered signaling related to IFN-γ induced filopodia formation is not driving the formation of FAs.

CONCLUSIONS

In this study, we transfected Cos-7 cells to express only part of the canonical IFN-γ receptor complex (IFNγR1, not IFNγR2), meaning that cells could bind IFN-γ but not transduce the signal. After exposing these IFNγR1-expressing Cos-7 cells to immobilized IFN-γ, we observed robust filopodia generation (both in number and in retention). The interaction between

https://dx.doi.org/10.1021/acs.bioconjchem.0c00105
Bioconjugate Chem. 2020, 31, 1362−1369

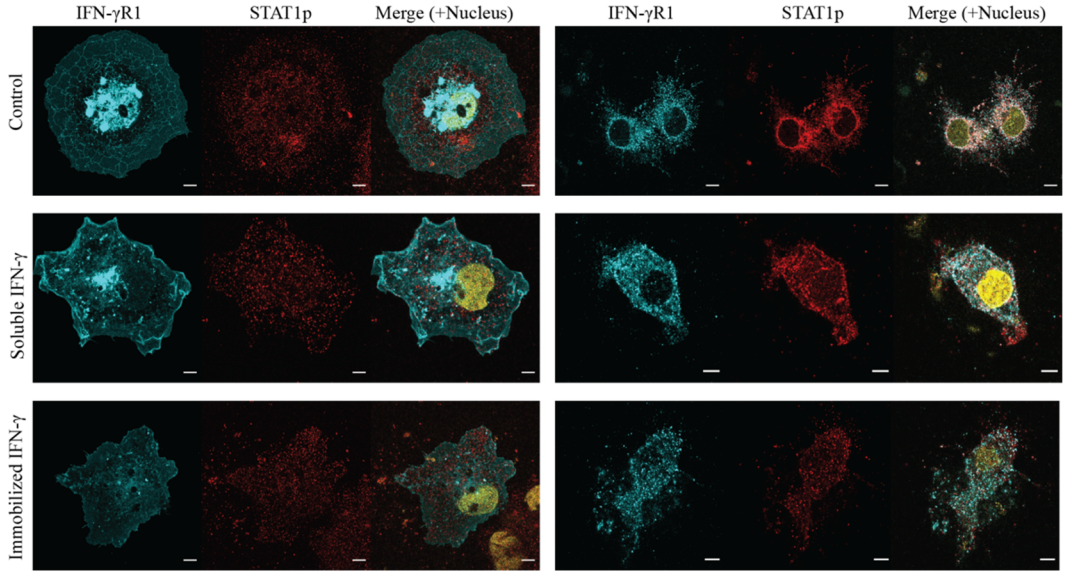

Figure 5. Exposure of IFNγR1-expressing Cos-7 to IFN-γ does not activate canonical signaling pathways. Confocal imaging at the basal surface of Cos-7 cells (left) and NSCs (right) following incubation on control (no IFN-γ) surfaces, with soluble ligand, or on immobilized IFN-γ surfaces. Representative Cos-7 cells show no apparent change in STAT1p levels based on treatment. Typical stimulated NSCs show STAT1p has nuclear localization (Hoeschst 33342, yellow) compared to control cells, as expected. Scale bars represent 10 μm.

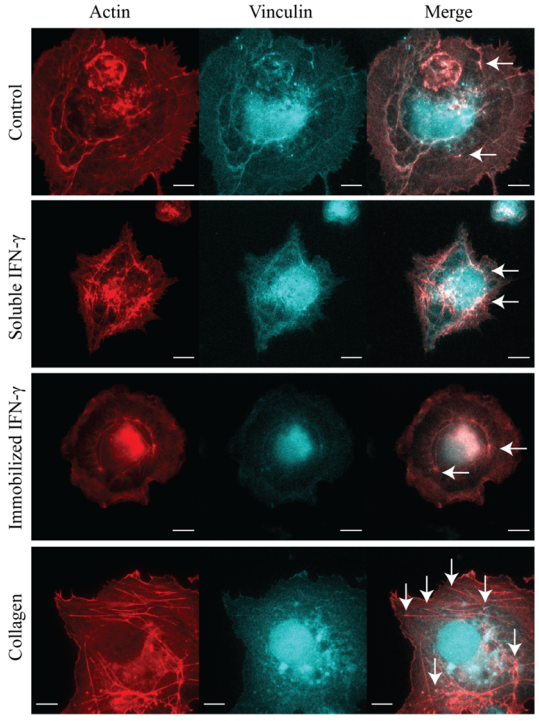

Figure 6. Immobilized IFN-γ does not generate focal adhesions. After exposing IFNγR1-expressing Cos-7 cells to IFN-γ in soluble and immobilized forms, there was no observed change in focal adhesion generation when compared to control cells, as seen in representative confocal images of the basal surface. Cells grown on collagen (bottom row) generated many FAs. White arrows indicate vinculin localization at the ends of actin stress fibers. Scale bars represent 10 μm.

IFN-γ and IFNγR1 was specific, and we did not observe any downstream pathway activation or generation of focal adhesions. This suggests that immobilized proteins activate a response which is dependent upon immobilization itself and independent of the canonical action of the protein.

The observation that immobilized and soluble versions of a signaling protein have different effects is not new, but typically this is investigated along the lines of its canonical response, e.g., that matrix-bound IFN-γ is more potent than soluble.[38] Here, we present a different finding: that the presentation of a protein (i.e., immobilized vs soluble) and its receptor can drive cell behaviors completely independent of canonical signaling pathways or FA-mediated substrate adhesion. This finding could have broad implications for the fields of tissue engineering/regenerative medicine and biomaterials design, where a common approach is to immobilize proteins to substrates in order to guide a specific cell behavior. While classically this approach is believed to improve latency, potency, and spatial patterning of signaling proteins, our work demonstrates that this is not the entire picture: the choice of immobilization strategy can intrinsically affect cell behavior. In the past, we have immobilized IFN-γ in order to drive neurogenesis from NSCs.[2−4,19] However, we have observed some unique behaviors that cannot be replicated with soluble IFN-γ: chiefly, the generation of nestin-expressing neurons[2] and the formation of neuroepithelium-like structures[4] with a regional identity following subcutaneous maturation.[17] In addition, we did not observe any migration of either Cos-7s or NSCs during time-lapse imaging so the robust filopodia generation on these nonmigratory cells may indicate a specialized function. Such filopodia exist but have been difficult to characterize thus far, since they share similar characteristics as migratory filopodia and still lack known molecular markers to distinguish them.[39] Specialized filopodia have been observed during sonic hedgehog signaling[40] and epidermal growth factor signaling,[41] and are typically involved in the transport of a soluble ligand. Our findings here suggest that the differences could be due to our immobilization strategy and alternate signaling pathways, rather than simply persistent canonical pathway activation, as the full signaling complex is not present in Cos-7 cells.

https://dx.doi.org/10.1021/acs.bioconjchem.0c00105
Bioconjugate Chem. 2020, 31, 1362−1369

EXPERIMENTAL PROCEDURES

Immobilized IFN-γ Surface Preparation. We adapted a protocol from a previous publication to prepare culture substrates.[9] We UV/ozone cleaned the glass bottom culture dishes (Mattek Corporation) before addition of any reagents. We added 3-(aminopropyl)-triethoxysilane (Sigma-Aldrich) diluted at 1:10 ratio in absolute ethanol to each dish and incubated for 2 h under a steady flow of nitrogen gas. We rinsed the surfaces with water and 70% ethanol to remove excess reagent. We then incubated them for 1 h with 62 μM dibenzocyclooctyne-*N*-hydroxysuccinimide ester (DIBO-NHS) in PBS. We stored control surfaces in fresh PBS at this point. For immobilized protein surfaces, we used additional PBS to rinse excess reagent. To prevent any nonspecific adsorption of azIFN-γ, we incubated surfaces with 1.5% BSA (w/v) in PBS for 30 min and washed with PBS prior to azIFN-γ incubation. We added azIFN-γ at a concentration of 600 ng/mL and incubated for 45−60 min before replacing it with fresh PBS for storage. Adsorbed conditions received no DIBO-NHS treatment and the same BSA/azIFN-γ treatment.

Extraction and Culture of Primary Neural Stem Cells. All procedures involving animals were approved by the University of Akron institutional animal care and use committee. We isolated NSCs from the SVZ of female Fisher 344 rats as described previously[2,42] and cultured them in growth medium as neurospheres. Prior to plating, we dissociated neurospheres by pipetting, counted, and plated individual cells at 10^5 cells/mL. We used passage 3−6 cells in all experiments.

Production of Recombinant Azide-Tagged IFN-γ. We produced and purified azide-tagged IFN-γ as described previously with no changes.[2]

Cos-7 Culture and Transfection. We carried out mammalian cell culture and transfection using standard protocols. We cultured Cos-7 cell lines in Dulbecco's Modified Eagle Medium (DMEM) supplemented with 10% fetal bovine serum and 1% penicillin−streptomycin until 70−90% confluency and seeded to 35 mm glass bottom culture dishes at 10^5 cells/mL 2 days prior to imaging. We passaged cells up to six times. To coat glass bottom dishes with collagen, we incubated them with a 35 μL/mL solution in PBS overnight at 4 °C. We transfected cells 18−24 h prior to imaging using Lipofectamine 2000 transfection reagent (Thermo Fisher Scientific). We purchased murine IFNγR1-GFPSpark plasmid from Sinobiological (Beijing, China). We exchanged DMEM for Opti-MEM I without phenol red for imaging and correlation experiments.

Total Internal Reflectance Fluorescence Imaging. We imaged cells on an inverted microscope (Eclipse Ti, Nikon Instruments, Tokyo, Japan) with a through the objective TIRF laser. TIRF allows for the excitation of fluorophores up to 60−100 nm from the glass surface negating the epifluorescence bulk signal.[43] For static imaging, we used NSCs or Cos-7 cells transfected with IFNγR1-GFPSpark plated at 10^5 cells/mL on surfaces with and without immobilized azIFN-γ and incubated them for 4 h. We stained the membrane of NSCs for 10 min with DiO-C18 dye and washed with imaging media. We excited IFNγR1-GFPSpark or DiO-C18 with a 488 nm solid state laser (Melles Griot, Carlsbad, CA) and detected the signal via CCD camera (Evolve 512, Photometrics, Tucson, AZ). We adjusted the laser angle by stepper motor to obtain TIR at the glass surface. For time-lapse imaging, we trypsinized Cos-7-expressing IFNγR1-GFPSpark from culture dishes and plated them on control or immobilized IFN-γ wells on the microscope stage. We collected time-lapse images on a landing/spreading cell every 30 s for up to 1 h.

Filopodia Quantification. We collected TIRF images for each group and subjected them to FiloQuant analysis using the open source ImageJ plugin.[25,26] Briefly, using the semi-automatic analysis, we cropped each cell image and adjusted so the region of interest was well-defined. We changed the following settings from the default analysis: threshold for cell edge = 25, holes on edges were not filled, threshold for filopodia = 35, and max distance from the cell edge = 40. Final images showed filopodia overlaid in purple, and those under 8 pixels (~1.2 μm) were manually excluded to remove false positives.

Fluorescence Correlation Spectroscopy. We performed FCS using a modified inverted microscope (Eclipse Ti, Nikon Instruments, Tokyo, Japan) as previously described.[44,45] Briefly, we focused a 488 nm laser at 300 nW power on the peripheral membrane area of a cell expressing murine IFNγR1-GFPSpark. We added soluble IFN-γ at a concentration of 150 ng/mL. We collected five 10 s acquisitions per cell to observe fluorescence intensity fluctuations over time. Photons were focused through a 50 μm pinhole to reduce scattering and recorded by a time correlated single-photon avalanche diode (SPAD) detector. We processed fluctuation records as described previously to obtain fluorescence auto-correlation curves fit to a single component two-dimensional diffusion model.[44,45] The characteristic lag time (τ_D) through the laser focus allows for calculation of diffusion of the receptor using $D_{eff} = \omega^2/4\tau_D$.

Dye Labeling of Recombinant IFN-γ. We incubated purifed IFN-γ with a 10 M excess of 5(6)-carboxy-X-rhodamine *N*-succinimidyl ester overnight at 4 °C. We removed excess dye by centrifugation in a Zeba desalting column (Thermo Scientific) which contains a size exclusion chromatographic resin retaining small molecules of <1000 Da. The labeling efficiency based on absorbance was 20−35% of total protein.

Fluorescence Cross-Correlation Spectroscopy. We performed FCCS on the same instrument as above, with these experiments using an additional 561 nm laser at 800 nW power and delayed 50 ns relative to the 488 nm laser. A second filter path and SPAD detector allows collection of the longer wavelength photons. We processed fluctuation records as above to obtain fluorescence auto-correlation curves for each fluorophore and a cross-correlation curve fit to a single component two-dimensional model. The fluctuations of the two species allow calculation of the correlation proportional to the codiffusion of species.

$$f_c = \frac{\langle N_{rg} \rangle}{\min[(\langle N_{rg} \rangle + \langle N_r \rangle), (\langle N_{rg} \rangle + \langle N_g \rangle)]}$$

Correlation values ideally range from zero to 1, indicating the fraction of fluorophores moving together through the laser focus. Values above 0.1 are considered to have a simple dimer tendency, and values above 0.2 are considered to have higher order oligomerization.[44]

Immunostaining and Confocal Imaging. We fixed Cos-7-expressing IFNγR1-GFPSpark or NSCs with 4% PFA for 30 min after 4 h of incubation on control and immobilized IFN-γ plates. Following a PBS wash, we permeabilized cells using

https://dx.doi.org/10.1021/acs.bioconjchem.0c00105
Bioconjugate Chem. 2020, 31, 1362−1369

0.1% Triton X-100 in PBS for 5 min and blocked with 10% FBS in PBS for 1 h. We incubated cells with primary antibodies overnight at 4 °C. We used rabbit anti-STAT1p (Tyr701, Invitrogen, 44-376G, 1:300 dilution), mouse anti-IFNγR1 (Santa Cruz Biotechnology, sc-12755, 1:400 dilution), and mouse anti-vinculin (7F9, Santa Cruz Biotechnology, sc-73614, 1:300 dilution). After washing with PBS, we incubated the NSCs with goat anti-mouse AlexaFluor 546 (Invitrogen, A11030, 1:400 dilution) and donkey anti-rabbit AlexaFluor 488 (Invitrogen, A21206, 1:400 dilution), while we incubated the Cos-7 with donkey anti-rabbit AlexaFluor 647 (Invitrogen, A31573, 1:400) for 1 h at 25 °C. For actin staining, during this step, we also added phalloidin-CF568 (Biotium, 00044, as per the manufacturer's protocol). Following washing with PBS, we stained nuclei with Hoechst 33342 (Invitrogen, 10 μM) for 7 min. Finally, we briefly washed the cells and mounted them (Invitrogen, ProLong Gold). We imaged the cells using a confocal microscope setup of four lasers of 358, 488, 561, and 647 nm.

Statistical Analyses. Outliers are displayed on the box plots as a red cross if the value is 1.5 times above or below the interquartile range. We performed statistical analyses using two-tailed Student's *t* tests assuming unequal variance in pairwise comparisons. We considered a *p*-value <0.05 to be significant.

■ ASSOCIATED CONTENT

Supporting Information

The Supporting Information is available free of charge at https://pubs.acs.org/doi/10.1021/acs.bioconjchem.0c00105.

Representative TIRF images of NSCs, Filoquant data output, and representative auto- and cross-correlation curves (PDF)

■ AUTHOR INFORMATION

Corresponding Authors

Adam W. Smith − *Department of Chemistry, The University of Akron, Akron, Ohio 44325, United States;* orcid.org/0000-0001-5216-9017; Email: asmith5@uakron.edu

Nic D. Leipzig − *Department of Biomedical Engineering and Department of Chemical, Biomolecular, and Corrosion Engineering, The University of Akron, Akron, Ohio 44325, United States;* orcid.org/0000-0002-6356-7691; Email: nl21@uakron.edu

Authors

Shaun M. Christie − *Department of Chemistry, The University of Akron, Akron, Ohio 44325, United States*

Trevor R. Ham − *Department of Biomedical Engineering, The University of Akron, Akron, Ohio 44325, United States*

Grant T. Gilmore − *Department of Chemistry, The University of Akron, Akron, Ohio 44325, United States*

Paul D. Toth − *Department of Chemistry, The University of Akron, Akron, Ohio 44325, United States*

Complete contact information is available at: https://pubs.acs.org/10.1021/acs.bioconjchem.0c00105

Author Contributions

‖S.M.C., T.R.H.: These authors contributed equally to this manuscript.

Notes

The authors declare no competing financial interest.

■ ACKNOWLEDGMENTS

The research presented here was supported by the National Science Foundation under grant number CHE-1753060 (S.M.C., G.T.G., P.D.T., and A.W.S.). This work was also partially supported by the National Institute of Neurological Disorders and Stroke (NINDS) (USA) under grant R21NS096571-01 (T.R.H. and N.D.L.).

■ REFERENCES

(1) Scott, J. D., and Pawson, T. (2009) *Science 326* (5957), 1220−1224.

(2) Ham, T. R., Farrag, M., and Leipzig, N. D. (2017) *Acta Biomater. 53*, 140−151.

(3) Leipzig, N. D., Xu, C., Zahir, T., and Shoichet, M. S. (2010) *J. Biomed. Mater. Res., Part A 93* (2), 625−633.

(4) Li, H., Koenig, A. M., Sloan, P., and Leipzig, N. D. (2014) *Biomaterials 35* (33), 9049−9057.

(5) DeForest, C. A., and Tirrell, D. A. (2015) *Nat. Mater. 14* (5), 523−531.

(6) McCormick, A. M., Jarmusik, N. A., and Leipzig, N. D. (2015) *Acta Biomater. 28*, 33−44.

(7) McCormick, A. M., Wijekoon, A., and Leipzig, N. D. (2013) *Bioconjugate Chem. 24* (9), 1515−1526.

(8) Offenhaeusser, A., Boecker-Meffert, S., Decker, T., Helpenstein, R., Gasteier, P., Groll, J., Moeller, M., Reska, A., Schaefer, S., Schulte, P., and Vogt-Eisele, A. (2007) *Soft Matter 3*, 290−298.

(9) Wilkinson, A. E., Kobelt, L. J., and Leipzig, N. D. (2014) *J. Biomed. Mater. Res., Part A 102* (10), 3419−3428.

(10) Yu, L. M., Kazazian, K., and Shoichet, M. S. (2007) *J. Biomed. Mater. Res., Part A 82* (1), 243−255.

(11) Matsuo, I., and Kimura-Yoshida, C. (2014) *Philos. Trans. R. Soc., B 369* (1657), 20130545.

(12) Barish, M. E., Mandorf, N. B., and Raissdana, S. S. (1991) *Dev. Biol. 144*, 412−423.

(13) Schroder, K., Hertzog, P. J., Ravasi, T., and Hume, D. A. (2004) *J. Leukocyte Biol. 75*, 163−189.

(14) Ramana, C. V., Gil, M. P., Schreiber, R. D., and Stark, G. R. (2002) *Trends Immunol. 23* (2), 96−101.

(15) Thiel, D. J., le Du, M. H., Walter, R. L., D'Arcy, A., Chene, C., Fountoulakis, M., Garotta, G., Winkler, F. K., and Ealick, S. E. (2000) *Structure 8* (9), 927−936.

(16) Walter, M. R., Windsor, W. T., Nagabhushan, T. L., Lundell, D. J., Lunn, C. A., Zauodny, P. J., and Narula, S. K. (1995) *Nature 376* (July), 230−235.

(17) Farrag, M., and Leipzig, N. (2018) *Cells 7* (10), 173.

(18) Kim, S. J., Son, T. G., Kim, K., Park, H. R., Mattson, M. P., and Lee, J. (2007) *Neurochem. Res. 32* (8), 1399−1406.

(19) Leipzig, N. D., Wylie, R. G., Kim, H., and Shoichet, M. S. (2011) *Biomaterials 32* (1), 57−64.

(20) Podolsky, M. A., Solomos, A. C., Durso, L. C., Evans, S. M., Rall, G. F., and Rose, R. W. (2012) *J. Neuroimmunol. 251* (1−2), 33−38.

(21) Wong, G., Goldshmit, Y., and Turnley, A. M. (2004) *Exp. Neurol. 187* (1), 171−177.

(22) Zahir, T., Chen, Y. F., MacDonald, J. F., Leipzig, N., Tator, C. H., and Shoichet, M. S. (2009) *Stem Cells Dev. 18* (10), 1423−1432.

(23) Fischer, R. S., Lam, P. Y., Huttenlocher, A., and Waterman, C. M. (2019) *Dev. Biol. 451* (1), 86−95.

(24) Aruffo, A. (2002) *Curr. Protoc. Mol. Biol. 60* (1), 16.12.1−16.12.7.

(25) Jacquemet, G., Paatero, I., Carisey, A. F., Padzik, A., Orange, J. S., Hamidi, H., and Ivaska, J. (2017) *J. Cell Biol. 216* (10), 3387−3403.

(26) Jacquemet, G., Hamidi, H., and Ivaska, J. In *Computer Optimized Microscopy: Methods and Protocols*; Rebollo, E., and Bosch, M., Eds.; Springer: New York, 2019; pp 359−373.

(27) Khalili, A. A., and Ahmad, M. R. (2015) *Int. J. Mol. Sci. 16*, 18149−18184.

(28) Marita, M., Wang, Y., Kaliszewski, M. J., Skinner, K. C., Comar, W. D., Shi, X., Dasari, P., Zhang, X., and Smith, A. W. (2015) *Biophys. J. 109* (9), 1937−1945.
(29) Huang, Y., Bharill, S., Karandur, D., Peterson, S. M., Marita, M., Shi, X., and Kaliszewski, M. J. (2016) *eLife 5*, 1−27.
(30) Lakowicz, J. R. *Principles of Fluorescence Spectroscopy*, 3rd ed.; Springer: Boston, 2006; pp 797−840.
(31) Comar, W. D., Schubert, S. M., Jastrzebska, B., Palczewski, K., and Smith, A. W. (2014) *J. Am. Chem. Soc. 136* (23), 8342−8349.
(32) Kanaoka, E., Nagata, S., and Hirano, K. (1999) *Int. J. Pharm. 188* (2), 165−172.
(33) Wood, W., and Martin, P. (2002) *Int. J. Biochem. Cell Biol. 34*, 726−730.
(34) Mattila, P. K., and Lappalainen, P. (2008) *Nat. Rev. Mol. Cell Biol. 9* (6), 446−454.
(35) Faix, J., Breitsprecher, D., Stradal, T. E. B., and Rottner, K. (2009) *Int. J. Biochem. Cell Biol. 41* (8−9), 1656−1664.
(36) Hoffmann, B., and Schafer, C. (2010) *Cell Adhes. Migr. 4* (2), 190−193.
(37) Bazan, J. F. (1990) *Proc. Natl. Acad. Sci. U. S. A. 87*, 6934−6938.
(38) Alvarado, J., Taylor, P., Castillo, J. R., and Thomas, L. E. (2005) *Immunol. Lett. 99* (1), 109−112.
(39) Fairchild, C. L., and Barna, M. (2014) *Curr. Opin. Genet. Dev. 27*, 67−73.
(40) Sanders, T. A., Llagostera, E., and Barna, M. (2013) *Nature 497* (7451), 628−632.
(41) Lidke, D. S., Lidke, K. A., Rieger, B., Jovin, T. M., and Arndt-Jovin, D. J. (2005) *J. Cell Biol. 170* (4), 619−626.
(42) Li, H., Wijekoon, A., and Leipzig, N. D. (2012) *PLoS One 7* (11), e48824.
(43) Mattheyses, A. L., Simon, S. M., and Rappoport, J. Z. (2010) *J. Cell Sci. 123*, 3621−3628.
(44) Kaliszewski, M. J., Shi, X., Hou, Y., Lingerak, R., Kim, S., Mallory, P., and Smith, A. W. (2018) *Methods 140−141*, 40.
(45) Jastrzebska, B., Comar, W. D., Kaliszewski, M. J., Skinner, K. C., Torcasio, M. H., Esway, A. S., Jin, H., Palczewski, K., and Smith, A. W. (2017) *Biochemistry 56*, 61−72.

https://dx.doi.org/10.1021/acs.bioconjchem.0c00105
Bioconjugate Chem. 2020, 31, 1362−1369